Korean J. Chem. Eng., 32(4), 761-766 (2015)
DOI: 10.1007/s11814-014-0300-3

pISSN: 0256-1115
eISSN: 1975-7220

Synthesis and thermal annealing treatment of octylphosphonic acid-capped CdSe-tetrapod nanocrystals for bulk hetero-junction solar cell applications

Nguyen Tam Nguyen Truong, Kieu Thanh Trinh, Viet Thanh Hau Pham, Chang Duk Kim, and Chinho Park†

School of Chemical Engineering, Yeungnam University, 280, Daehak-ro, Gyeongsan 712-749, Korea
(*Received 10 June 2014 • accepted 5 October 2014*)

Abstract−CdSe-tetrapod nanocrystals (NCs) were synthesized by using octylphosphonic acid (OPA) as a capping ligand and cadmium oxide (CdO) as a cadmium precursor. The effects of thermal annealing in nitrogen (N_2) environment on the chemical composition, morphology, crystal structure and optoelectronic properties of the CdSe-tetrapods have been investigated. Remarkable difference in the morphological and optoelectronic properties between as-synthesized and N_2-annealed CdSe NCs was observed. The photoluminescence (PL) peak of N_2-annealed CdSe NCs shifted to lower energy and UV-vis absorption spectra shifted to longer wavelength, indicating the size increase and improvement of the crystallinity of the CdSe tetrapods. The power conversion efficiency of bulk hetero-junction solar cells made with the annealed CdSe NCs showed higher value compared with the efficiency of cells made with as-synthesized CdSe NCs.

Keywords: Photoluminescence, Absorption, Red-shift, Surface Roughness, CdSe, Bulk Hetero-junction Solar Cells

INTRODUCTION

Colloidal inorganic nanocrystals have attracted broad interest because of sensitive size-dependent electrical, morphological, and optical properties [1-4]. Controlling a nanocrystal's shape is important in catalysis, light emitting diodes, biological labeling, and photovoltaics [5-9]. One promising shape-control technique, hot-injection synthesis, produces high quality nanocrystals that can be easily tailored into desired particle shape and size (and thus the band gap) by changing the synthesis conditions such as precursor type, growth temperature, and growth time [10], and this technique paves the way to new geometries and shape-dependent properties of semiconductor nanoparticles. From this technique, a variety of shapes of CdSe particles (spherical, hexagonal nanorods, nanowires, nanoneedles, and tetrapods) have been synthesized [11]. However, the simultaneous control of the morphology, shape, and size distribution of semiconductor nanocrystals is challenging. Size-dependent optical properties are probably the most attractive property of CdSe NCs, and it is possible to control variously sized CdSe NCs that emit blue to red color with high quality. The width and intensity of PL spectra of CdSe NCs are important, because they are very sensitive to features such as size, shape, surface impurities, and defects in nanoparticles.

CdSe NCs have been applied in bulk hetero-junction (BHJ) solar cells because of their potential versatility to achieve high power conversion efficiency due to enhanced electron transport [12]. For BHJ solar cells, the shape and size of CdSe nanocrystals are very important in enhancing carrier transport. The impurities remaining at synthesized CdSe NCs could affect the electron transport of the CdSe leading to decreased short circuit current density and efficiency of the BHJ solar cells [11]. By thermal annealing, the optical property and structural transformation of the CdSe nanocrystals can be improved [11].

The optical property of CdSe nanocrystals is very important in hybrid BHJ solar cells, and it can be characterized from the wavelength and line width of the ultraviolet visible (UV-vis) and photoluminescence (PL) spectra, since the UV-vis and PL properties are very sensitive to the nanoparticle's size, shape and surface [10].

In this work, we synthesized high quality CdSe-tetrapod nanocrystals and investigated the influence of thermal annealing treatment in N_2 environment of as-synthesized OPA-capped CdSe nanotetrapods on their optical, chemical composition and morphological properties. Additionally, the effects of annealing on the BHJ solar cell performance have been studied.

EXPERIMENTAL

CdSe tetrapods (Tpods) nanocrystals were synthesized using a method reported elsewhere [12]. In detail, 0.7 g of cadmium oxide (CdO), 5.2 g of trioctylphosphonic acid (TOP), and 2.14 g of octylphosphonic acid (OPA) were heated to 300 °C in a two-necked flask under a nitrogen (N_2) flow. When the cadmium solution turned colorless, heat was removed, and the solution was kept under a nitrogen flow. The selenium precursor was prepared by mixing 0.84 g of selenium (Se) with 2.54 g of tributylphosphine (TBP) in 0.6 mL of toluene and cooled in a refrigerator for 20 min prior to the injection. After 48 hour, the cadmium precursor was reheated to 300 °C, and the selenium precursor was injected rapidly at 300 °C. The tetrapods were grown at 250 °C for 50 min. The synthesized CdSe tetrapods were washed five times with a mixture of toluene and ethanol to remove the excess capping ligands and centrifuged five times.

†To whom correspondence should be addressed.
E-mail: chpark@ynu.ac.kr

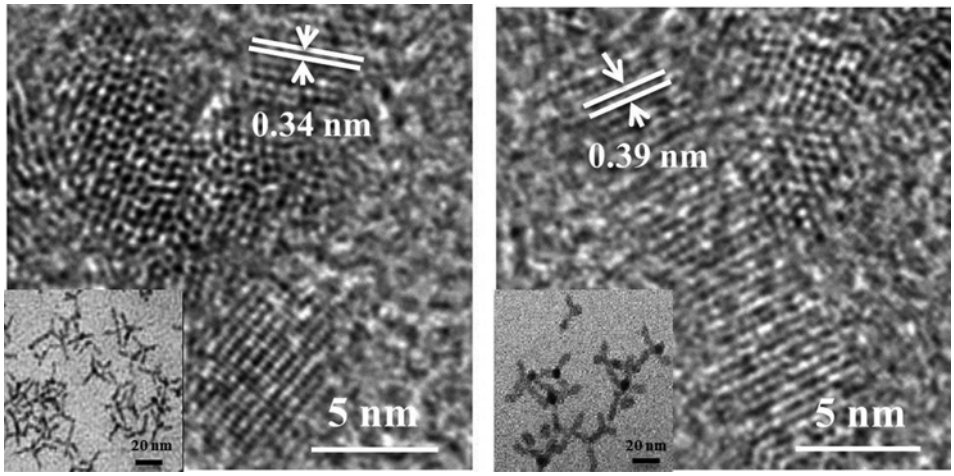

Fig. 1. HR-TEM and TEM (inserts) images of (a) as-synthesized and (b) N_2-annealed at 350 °C CdSe Tpod nanocrystals.

Ultraviolet-visible (UV-vis), photoluminescence (PL), X-ray diffraction (XRD) and transmission electron microscopy (TEM) were used to characterize the structural and optical properties of the CdSe nano-tetrapod particles. The UV-vis (Cary 5000) spectra of ligand-capped CdSe tetrapod nanoparticles were obtained using 1.0 cm path length quartz cells. The samples were prepared by dispersing the nanoparticles in ethanol prior to the measurements. The photoluminescence (PL) was measured with a custom-made PL system at room temperature using 488 nm (argon laser) as the excitation source. The size and shape of the NCs were estimated with a high-resolution transmission electron microscope (HR-TEM, H-7600). X-ray photoelectron spectroscopy (XPS) was used to characterize the optical properties and chemical compositions of the CdSe nanocrystals. The surface morphology of the active layers was investigated by atomic force microscopy (AFM).

BHJ solar cells having the structure of glass/ITO/PEDOT : PSS/CdSe-PCPDTBT/Al were then fabricated. A thin (~70 nm) layer of polyethylenedioxythiophene doped with polystyrene-sulfonic acid (PEDOT : PSS, Sigma Aldrich) was spin-coated at 4,000 rpm for 30 s onto the cleaned indium tin oxide (ITO)-coated glass substrates and dried at 100 °C for 30 min by using the hotplate placed inside the N_2 glove box. The suspension of CdSe nanoparticles and poly[2,6-(4,4-bis(2-ethylhexyl)-4H-cyclopenta[2,1-b;3,4-b']-dithiophene)-alt-4,7-(2,1,3-benzothiadiazole)] [PCPDTBT] polymer was dropped and spin-coated onto the preformed PEDOT : PSS layers at 4,000 rpm for 30 s to form 150±5 nm-thick photoactive CdSe-PCPDTBT bulk hetero-junction layers. The samples were then dried at 140 °C for 30 min. Finally, a 100 nm-thick aluminum (Al) electrode was added to the top of the films by thermal evaporation to complete the devices. All the device fabrication processes were performed in a glove box under nitrogen environment. The solar cells' current density-voltage (J-V) characteristics were investigated both in the dark and under AM1.5G illumination by a solar simulator (Keithley 69911).

RESULTS AND DISCUSSION

Figs. 1(a) and 1(b) show HR-TEM and TEM (inserted) images of the CdSe Tpods nanocrystals (NCs). A large fraction of branches was obtained without selective precipitation, which shows that the tetrapod had formed corresponding to the (002) planes for the Wurtzite structure of CdSe [13,14]. Fig. 1(a) and the inset show that the tetrapod limbs were approximately ~26 nm long and the lattice fringes of the CdSe Tpods with fringe spacing of 0.34 nm. OPA-capped CdSe Tpods nanocrystals were synthesized, and the nanoparticles were annealed at 350 °C in nitrogen environment. Fig. 1(b) with inserted image shows the tetrapod limbs were approximately ~27 nm long and the lattice fringes of the CdSe Tpods with fringe spacing of 0.39 nm. After annealing, the nanoparticles were clearly segregated with a little increase in the particle size (~1 nm) and in the fringe spacing (~0.05 nm), respectively. The lattice fringes were clearly visible, and no dislocation inside the nano-tetrapods was observed, confirming that the CdSe Tpods obtained in this study are highly crystalline in nature.

Fig. 2 shows the XRD patterns of as-synthesized and N_2-annealed

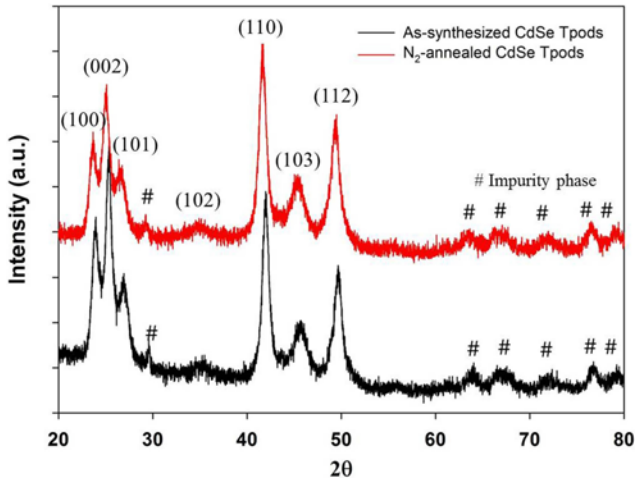

Fig. 2. The X-ray diffraction patterns of as-synthesized and N_2-annealed at 350 °C CdSe tetrapods with the reference peak positions of bulk Wurtzite CdSe crystal planes (ICDD-JCPDS: CdSe # 00-019-0191) displayed.

CdSe Tpods. The as-synthesized CdSe Tpods have hexagonal Wurtzite structure ((ICDD-JCPDS: CdSe #00-019-0191) [15] with 2θ peaks at 25, 43, 45 and 51° corresponding to the (002), (110), (103) and (112) crystal planes. The N_2-annealed CdSe Tpod nanocrystals have the same hexagonal Wurtzite structure, but the peaks are shifted toward lower 2θ values. The XRD pattern of the sample N_2-annealed at 350 °C showed a decrease in the full width at half maximum (FWHM) of the diffraction peaks, and the lattice fringe spacing is increased from ~0.345 nm (as-synthesized CdSe) to ~0.386 nm (N_2-annealed CdSe), an indication of an enhancement in the crystallinity and nanocrystals' grain sizes [11]. These results are consistent with the HR-TEM results, which showed a clear hexagonal structure [16-18].

The effects of thermal treatment on the nanoparticles' optical properties were studied by UV-vis and PL spectroscopy. Fig. 3 shows the absorption edges of the UV-vis spectra shifted towards longer wavelength from 565 nm to 578 nm, and the PL emission peaks shifted to smaller energies from 2.08 eV to 2.06 eV, as shown in Fig. 4. The red-shifting of the absorption edge and the emission peak due to sintering effects indicate an increasing of the nanoparticles' size. This result is consistent with the TEM measurements. The effects of air-annealing on the PL spectra of CdSe nanoparticles have been studied by Alivisatos et al. [19,20]. They reported that oxygen reacts with CdSe nanocrystals with the possible formation of surface CdO and SeO_2, and this oxygen will affect the PL intensity [21]. The influence of oxygen on the PL enhancement of CdSe was studied by Allen J. Bard et al. [22], who reported that the PL enhancement after thermal treatment in the air at 250 °C can be attributed to the combined effect of the crystallinity improvement and the surface passivation of CdSe NCs by surface oxides [23]. In our study, the PL intensity did not change very much, but the peak was shifted to a smaller energy. It is believed that the oxygen was removed after annealing at 350 °C in N_2 environment, and the crystallinity was improved, which we confirmed by XPS measurements.

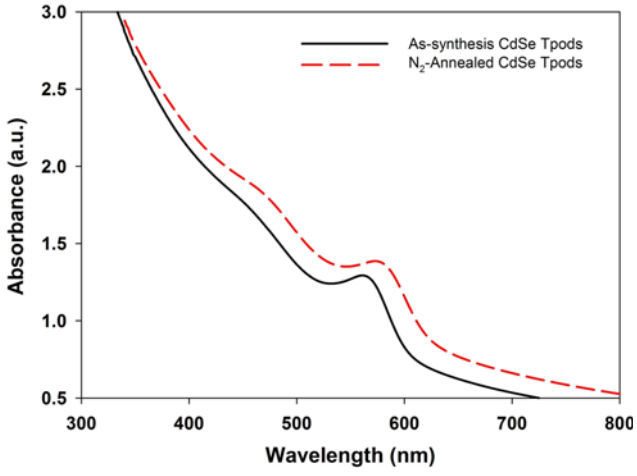

Fig. 3. UV-Vis absorption spectra of as-synthesized and N_2-annealed at 350 °C CdSe Tpod nanocrystals.

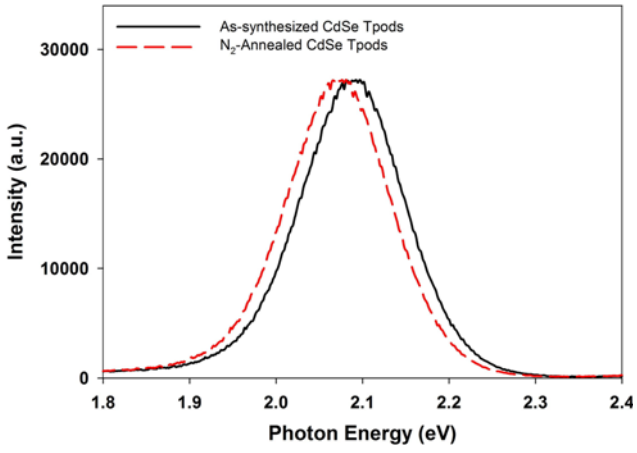

Fig. 4. Photoluminescence spectra of as-synthesized and N_2-annealed at 350 °C CdSe Tpod nanocrystals.

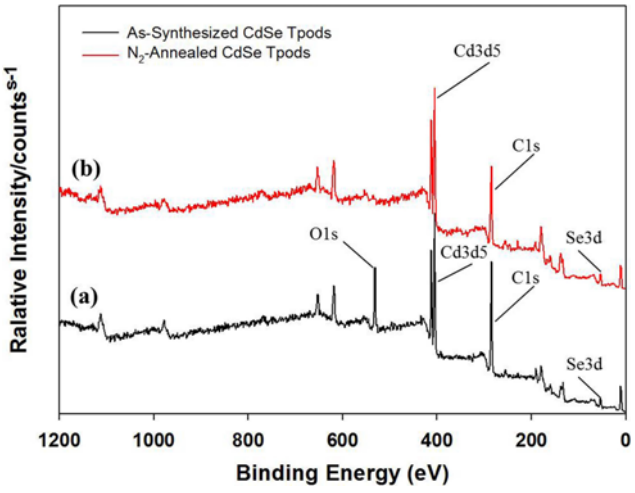

Fig. 5. XPS spectra of CdSe Tpod nanocrystals: (a) As-synthesized and (b) N_2-annealed at 350 °C.

The influence of thermal annealing on the CdSe Tpods' chemical bonding was investigated by XPS (Fig. 5). The general survey spectrum shows mainly the peaks of Cd and Se from nanocrystals, and the O and C peaks are also present. The survey spectrum of as-synthesized CdSe and N_2-annealed CdSe TPods shows the characteristic peaks in close position of bulk values [24]. Fig. 5(a) shows the XPS spectrum of as-synthesized CdSe Tpods, and the O 1s peak in the spectrum is attributed to the Se oxide (SeO_2) and cadmium oxide (CdO) formed on the surface of CdSe Tpods. After annealing, there is no O 1s peak, shown as in Fig. 5(b). This result confirms that the oxygen was removed by annealing at 350 °C in N_2 environment. However, in all our samples, SeO_x and CdO peaks are not presented, indicating that Se surface sites are not oxidized and our nano-tetrapods are relatively superior in quality.

Table 1. Binding energies of as-synthesis and N_2-annealed at 350 °C CdSe Tpods measured from the corresponding Cd 3d and Se 3d spectra (unit: eV)

Sample	Se 3d	Cd $3d_{5/2}$
As-synthesized CdSe Tpods	53.24 eV	404.82 eV
N_2-annealed CdSe Tpods	53.80 eV	405.22 eV

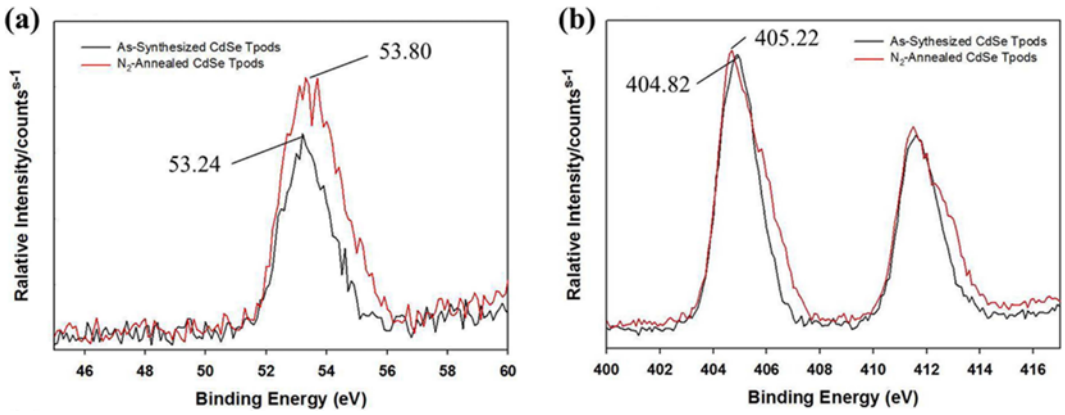

Fig. 6. (a) XPS spectrum corresponding to the Se 3d core region from differently prepared CdSe Tpod nanocrystals and (b) XPS spectrum corresponding to the Cd 3d core region from differently prepared CdSe Tpod nanocrystals.

High resolution XPS spectra of the as-synthesized and N_2-annealed CdSe Tpods were also recorded to reveal the detailed nature of the peaks (Fig. 6). The binding energies of as-synthesized and N_2-annealed CdSe Tpods NCs are listed in Table 1, and the corresponding Cd 3d, Se 3d peaks are shown in Fig. 6(a) and 6(b). The Se 3d XPS spectra (Fig. 6(a)) show the Se 3d peak of as-synthesized CdSe NCs at 53.24 eV being shifted to higher binding energy of 53.80 eV of N_2 annealed CdSe NCs. The Cd $3d_{5/2}$ peaks at 404.82 eV and 405.22 eV

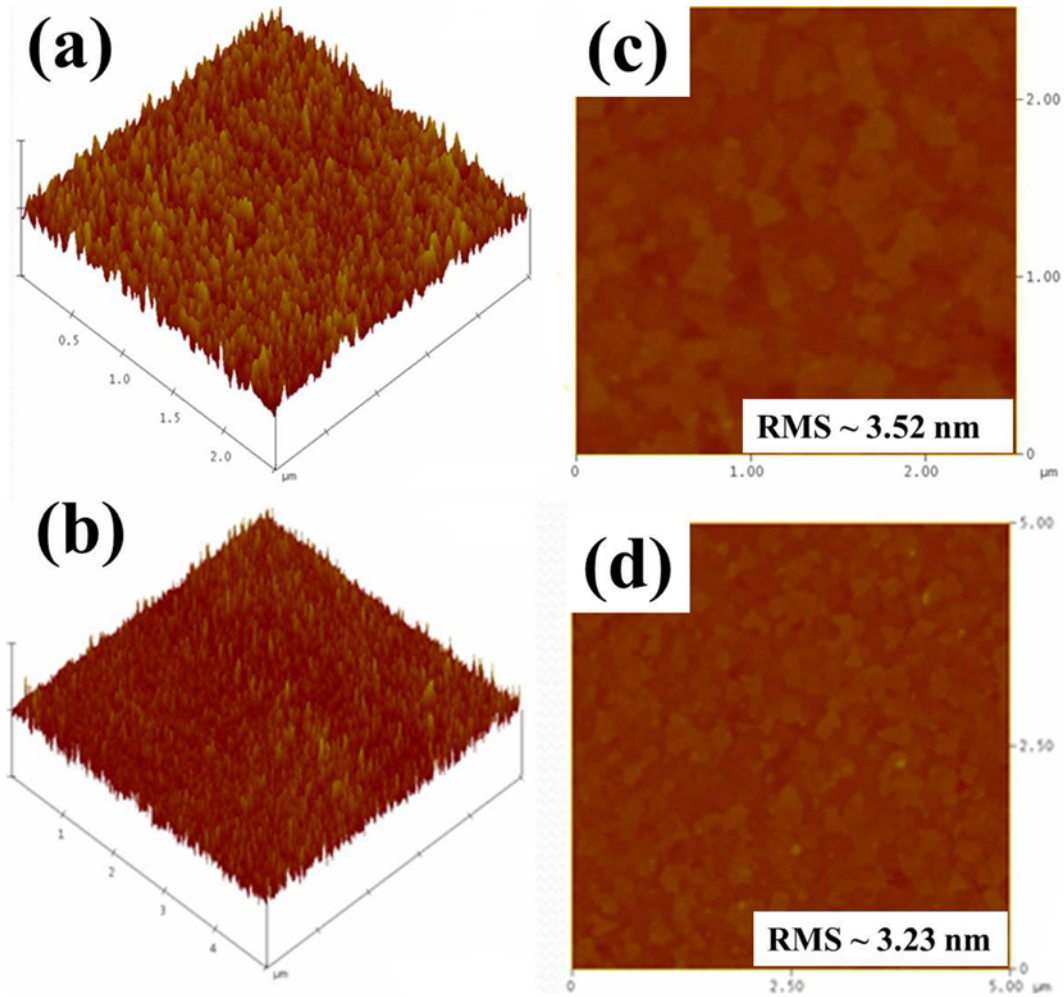

Fig. 7. AFM images and surface roughness (RMS) values of the (CdSe+PCPDTBT) active layer with as-synthesized (a), (c) and N_2-annealed CdSe tetrapod nanocrystals (b), (d).

that emerged after thermal annealing at 350 °C under nitrogen environment of as-synthesized CdSe NCs. After annealing, the binding energy was shifted to higher binding about 0.56 eV, and the intensity of Cd 3d levels increased, indicating that the formation of stronger bonding within the CdSe NCs (as shown in Fig. 6(b)). The presence of C 1s at ~282 eV was also identified [25]. These peaks and the absence of the peaks near 60 eV further confirm the presence of pure CdSe NCs phase [26,27]. The XPS data shown in this investigation further confirm the absence of cadmium oxide, hydroxide, and selenium oxide, indicating that high-purity CdSe Tpod nanocrystals are obtained after annealing in a nitrogen environment.

The influence of the thermal annealing of CdSe NCs on the formation of the device active layer and device performance were investigated. Fig. 7 shows the AFM images of the surface roughness morphologies of the solar cell devices. Fig. 7(a) and 7(c) show topography and three-dimensional (3D) AFM phase images of as-synthesized CdSe NCs samples, and the root mean square (RMS) roughness was 3.52 nm. Fig. 7(b) and 7(d) show topography and three-dimensional (3D) AFM phase images of N_2-annealed CdSe NCs samples, and the (RMS) roughness was 3.23 nm. The surface roughness indicates the degree of self-organization of a polymer, and devices demonstrate higher photovoltaic efficiency on the smooth surface than on the rough surface [28]. In this study, the surface roughness of the active layer is both smooth and homogeneous; however, the surface roughness of the photoactive layer formed with N_2-annealed sample was found to be smoother than that of as-synthesized sample.

Bulk hetero-junction solar cells of the structure, ITO (180 nm)/PEDOT : PSS (70 nm)/(CdSe+PCPDTBT) (150 nm)/Al (100 nm) were fabricated by using a blend of CdSe NCs (both as-synthesized and N_2-annealed) and PCPDTBT polymer in the chlorobenzene as a solvent, and the device parameters were measured under AM1.5G conditions. Devices were fabricated by using an optimized condition under nitrogen environment in a glove box. Power conversion efficiency of the cells made of as-synthesized CdSe NCs turned out to be ~1.52% (short-circuit current density (J_{sc}): 3.4 mA/cm^2), whereas for the cells made of N_2-annealed CdSe NCs at otherwise the same condition was ~2.2% (J_{sc}: 4.6 mA/cm^2), as shown in Fig. 8. On the other hand, the open-circuit voltage (V_{oc}: ~0.675) and the fill factor (FF: 0.61~0.67) were only slightly different. It is believed that the quality of the NCs was improved upon thermal annealing in N_2 environment, and the enhanced electron transport due to high-quality nanoparticles is crucial for the performance of PCPDTBT polymer-CdSe nanocrystal based BHJ solar cells. The short circuit current densities of the devices fabricated in this study appeared to be still limited. We believe that the bi-continuous interpenetrating percolation networks are not well constructed in the active layer of this study. Device efficiencies in this study are still low without any post-annealing, compared with those of reported BHJ solar cells made with CdSe Tpods NCs and low band gap polymer [12]. We believe that the relatively lower efficiencies observed in this study are partially attributed to the poorer carrier collection caused by the absence of optimized post-annealing process, which may lead to poorer interfacial contacts between the CdSe NCs and PCPDTBT polymer, creating a phase separation within the device active layer. We strongly believe that thermal annealing had a positive effect on the fabrication of BHJ solar cells, especially in the N_2-annealing case. The findings of this investigation could be useful in the development of BHJ-type or similar type thin film solar cells.

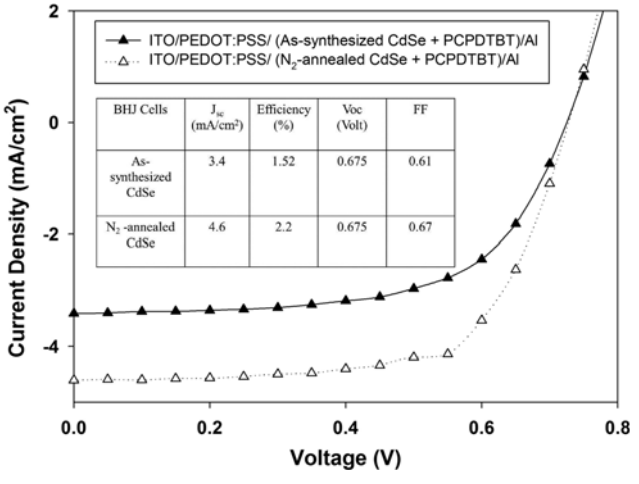

Fig. 8. J-V curves for the solar cells fabricated with as-synthesized and N_2-annealed CdSe tetrapod nanocrystals (CdSe/[CdSe+PCPDTBT]=0.7).

CONCLUSIONS

Semiconducting CdSe Tpods NCs were synthesized and annealed at 350 °C in a nitrogen environment. After annealing, the size of nanoparticles and grain size slightly increased. Additionally, the annealing in nitrogen red-shifts the PL and UV-vis absorption spectra, indicating the improvement of optical properties of nano-tetrapods and modification of the morphological, structural, and chemical composition of highly luminescent CdSe tetrapods NCs. The as-synthesized and N_2-annealed nanoparticles were applied to BHJ solar cells performance, demonstrating a potential to open a new way to improve the device performance.

ACKNOWLEDGEMENTS

This work was supported by the New & Renewable Energy Program (No. 20133030011330) and the Human Resources Development Program (No. 20124030200100) of the Korea Institute of Energy Technology Evaluation and Planning (KETEP) grant funded by the Korean Ministry of Trade, Industry and Energy (MOTIE).

REFERENCES

1. X. G. Peng, L. Manna, W. D. Yang, J. Wickham, E. Scher, A. Kadavanich and A. P. Alivistos, *Nature*, **404**, 59 (2000).
2. A. P. Alivistos, *Science*, **271**, 933 (1996).
3. L. E. Brus, *J. Chem. Phys.*, **90**, 2555 (1986).
4. Y. W. Jun, Y. Y. Jung, J. Cheon and V. Bulovic, *Nature*, **420**, 800 (2002).
5. T. S. Ahmadi, Z. L.Wang, T. C. Green, A. Henglein and A. Elsayed, *Science*, **272**, 1924 (1996).
6. M. C. Schlamp, X. G. Peng and A. P. Alivistos, *J. Appl. Phys.*, **82**,

5837 (1997).
7. W. C. W. Chan and S. M. Nie, *Science*, **281**, 2016 (1998).
8. W. U. Huynh, J. J. Dittmer and A. P. Alivistos, *Science*, **295**, 2425 (2002).
9. N. T. N. Truong and C. Park, *J. Japn. Appl. Phys*., **51**, 10NE27 (2012).
10. C. B. Murray, D. J. Norris and M. G. Bawendi, *J. Am. Chem. Soc*., **115**, 8706 (1993).
11. U. Farva and C. Park, *Sol. Energy. Mater. Sol. Cells*, **94**, 303 (2010).
12. S. Dayal, N. Kopidakis, D. Olson, D. S. Ginley and G. Rumbles, *Nano Lett*., **10**, 239 (2010).
13. H. Lee, S. W. Yoon, J. P. Ahn, Y. D. Suh, J. S. Lee, H. Lim and D. Kim, *Sol. Energy. Mater. Sol. Cells*, **93**, 779 (2009).
14. N. T. N. Truong, T. P. N. Nguyen and C. Park, *International J. Photoenergy*, **Article ID 146582**, 7 (2013), DOI:10.1155/2013/146582.
15. P. T. Chou, C. Y. Chen, C. T. Cheng, S. C. Pu, K. C. Wu, Y. M. Cheng, C. W, Lai, Y. H. Chou and H. T. Chiu, *J. Chem. Phys. Phys. Chem*., **7**, 222 (2006).
16. W. W. Yu, Y. A. Wang and X. G. Peng, *Chem. Mater*., **15**, 4300 (2003).
17. Q. Pang, L. J. Zhao, Y. Cai, D. P. Nguyen, G. Bastard and J. N. Wang, *Chem. Mater*., **17**, 5263 (2005).
18. Y. M. Jun, S. M. Lee, N. J. Kang and J. Cheon, *J. Am. Chem. Soc*., **123**, 5150 (2001).
19. J. E. B. Katari, V. L. Colvin and A. P. Alivisatos, *J. Phys. Chem*., **98**, 4109 (1994).
20. A. P. Alivisatos, *J. Phys. Chem*., **100**, 13226 (1996).
21. J. K. Lorenz and A. B. Ellis, *J.Am. Chem. Soc*., **120**, 10970 (1998).
22. N. Myung, Y. Bae and A. J. Bard, *Nano Lett*., **3**, 947 (2003).
23. M. Kuno, J. K. Lee, B. O. Dabbousi, F. V. Mikulec and M. G. Bawendi, *J. Chem. Phys*., **106**, 9869 (1997).
24. C. J. Vesely and D. W. Langer, *Phys. Review B*, **4**, 451 (1971).
25. C. D. Wangner, *Handbook of X-ray Photoelectron Spectroscopy*, Perkin-Elmer, Eden Prairie, MN (1979).
26. D. P. Masson, D. J. Lockwood and M. J. Graham, *J. Appl. Phys*., **82**, 1632 (1997).
27. Q. Yang, K. Tang, F. Wang, C. Wang and Y. Quian, *Mater. Lett*., **57**, 3508 (2003).
28. N. Hoth, P. Schilinsky, S. A. Choulis and C. J. Brabec, *Nano Lett*., **8**, 2806 (2008).